Controlling high-Q trapped modes in polarization-insensitive all-dielectric metasurfaces

Andrey Sayanskiy,[1] Anton S. Kupriianov,[2] Su Xu,[3,4] Polina Kapitanova,[1] Victor Dmitriev,[5] Vyacheslav V. Khardikov,[6,7] and Vladimir R. Tuz[3,4,7,*]

[1]*ITMO University, St. Petersburg 197101, Russia*

[2]*College of Physics, Jilin University, 2699 Qianjin St., Changchun 130012, China*

[3]*State Key Laboratory of Integrated Optoelectronics, College of Electronic Science and Engineering, Jilin University, 2699 Qianjin St., Changchun 130012, China*

[4]*International Center of Future Science, Jilin University, 2699 Qianjin St., Changchun 130012, China*

[5]*Electrical Engineering Department, Federal University of Para, PO Box 8619, Agencia UFPA, CEP 66075-900 Belem, Para, Brazil*

[6]*School of Radio Physics, V. N. Karazin Kharkiv National University, 4 Svobody Sq., Kharkiv 61022, Ukraine*

[7]*Institute of Radio Astronomy of National Academy of Sciences of Ukraine, 4 Mystetstv St., Kharkiv 61002, Ukraine*

(Received 29 November 2018; revised manuscript received 30 January 2019; published 15 February 2019)

We reveal peculiarities of the trapped (dark) mode excitation in a polarization-insensitive all-dielectric metasurface, whose unit supercell is constructed by particularly arranging four cylindrical dielectric particles. Involving group-theoretical description we discuss in detail the effect of different orientations of particles within the supercell on characteristics of the trapped mode. The theoretical predictions are confirmed by numerical simulations and experimental investigations. Since the metasurface is realized from simple dielectric particles without the use of any metallic components, they are feasibly scalable to both μm- and nanometer-size structures, and they can be employed in flat-optics platforms for realizing efficient light-matter interaction for multiple hot-spot light localization, optical sensing, and highly efficient light trapping.

DOI: 10.1103/PhysRevB.99.085306

I. INTRODUCTION

Today, with the advancements of nanotechnology, the science and engineering of subwavelength light-matter interactions move to design and fabrication of nanostructures with desired optical properties [1]. It allows one to construct optical components with previously unattainable characteristics. These also include planar metamaterials (metasurfaces) made of metallic (plasmonic) particles, which are extremely important parts of sensors, slow light and beam steering devices, holographic displays, near-IR tunable filters, fast optical interconnectors, switchers, and amplitude modulators.

A particular class of novel metasurfaces based on dielectric nanoparticles has several significant advantages compared to plasmonic ones, especially concerning their low losses and fabrication techniques targeting to higher frequencies of operation [2,3]. They are so-called all-dielectric [4,5] metasurfaces composed of subwavelength dielectric particles made of high-refractive-index material [6]. The particles are arranged into a lattice where each particle behaves as an individual resonator [7] sustaining a set of electric and magnetic dipolar and multipolar modes (referred to as Mie-type modes [8]). An appearance of these modes can be spectrally controlled and engineered independently [9,10].

Due to the unique features of optically induced electric and magnetic Mie-type modes of the dielectric particles, the all-dielectric metasurfaces are expected to complement or even replace different plasmonic components in a range of potential applications [11–13]. Among the variety of known metamaterial configurations supporting Mie-type modes we further distinguish a particular class of planar resonant structures, which allow obtaining the strongest resonant response due to excitation of so-called trapped (dark) modes [14–18]. Access to trapped modes of dielectric resonators may allow obtaining deeper subwavelength thicknesses while providing a sharp resonant response. In the electromagnetic theory [19], the trapped modes are considered as some degenerate states that are not directly coupled to the field of incoming radiation, whereas they can be excited indirectly by removing the degeneracy.

In particular, in order to lift the degeneracy and realize a necessary coupling of an incoming radiation with a trapped mode, some structural asymmetry can be introduced into the particles forming the metasurface [20,21] (recently, the trapped modes in such asymmetrical structures were referred to the phenomenon of bound states in the continuum (BIC) originated from distortion of the symmetry-protected bound state in the continuum [22,23]). As a side effect of the method, the resulting metasurface composed of asymmetrical particles becomes polarization sensitive even for a normally incident electromagnetic wave. This reduces the practical applicability of the metasurfaces based on trapped modes. In order to overcome this drawback, several designs of the metasurfaces composed of thin metallic particles have been proposed [24–31], whereas for the all-dielectric metasurfaces they are quite rare [32–34]. This is due to a greater flexibility available in designs of thin metallic resonators. They can be given a rather complicate shape that provides a specific configuration of the surface currents flow, which is impossible to realize

*tvr@jlu.edu.cn

in the volumetric dielectric resonators for the displacement (polarization) currents. Therefore, in order to access a trapped mode in polarization-insensitive all-dielectric metasurfaces another approach should be applied.

As such a design of polarization-insensitive all-dielectric metasurfaces [33], a multilayer configuration of dielectric resonators can be mentioned. In this configuration, in order to access a trapped mode, two additional scatterers of a particular form are attached diagonally to the upper and lower sides of the resonators forming metasurface. A multistep lift-off and deposition procedure is suggested for the resonators fabrication. While the metasurfaces consisting of ordinary (single-layer) asymmetric particles are fabricated and investigated [33], the structure composed of the multilayer resonators has been investigated only numerically. Apparently this is due to the fact that the technology of their production, although feasible, is quite complex.

Alternatively, a trapped mode can be excited in the polarization-insensitive metasurfaces whose unit cell comprises several particles arranged specifically (so-called supercell [35–39]). Although these metasurfaces possess a more complicated unit cell, their production complexity is the same as for the metasurfaces based on the ordinary single-particle unit cells.

Following the concept of supercell metasurfaces, in the present paper we employ group-theoretical predictions [40,41], numerical simulations, and experimental study for both far-field and near-field characteristics to reveal conditions of the trapped mode excitation in a polarization-insensitive metasurface. We distinguish several supercell's designs, which provide efficient coupling of the all-dielectric metasurface with a linearly polarized incident wave via the trapped mode. They utilize particles with a short coaxial-sector notch made in a form of smile since they can efficiently support the trapped mode [17].

II. THEORETICAL DESCRIPTION

For comparison purposes, we start our discussion with the demonstration of an electromagnetic response of the metasurface whose supercell is composed of solid disks (disks without notches). We consider that the metasurface under study is illuminated by a normally incident ($\vec{k} = \{0, 0, k_z\}$) linearly polarized wave with the electric field vector directed either along the x axis ($\vec{E} = \{E_x, 0, 0\}$, x-polarized wave) or along the y axis ($\vec{E} = \{0, E_y, 0\}$, y-polarized wave) (see Fig. 1).

The numerical simulations of the electromagnetic response of the metasurface were performed with the use of RF module of commercial COMSOL Multiphysics® finite-element electromagnetic solver. The Floquet-periodic boundary conditions were imposed on four sides of the unit cell to simulate the infinite two-dimensional array of resonators [42].

In the frequency band of interest there is only one resonant state, which corresponds to excitation of the lowest-order (dipole) electric mode (Mie-type resonance) [Fig. 2(a)]. This resonance is insensitive to the wave polarization, and can be related to the hybrid $EH_{11\delta}$ mode of an individual cylindrical dielectric resonator [12,17]. This resonance is distinguished on the spectral curves by the gray arrows.

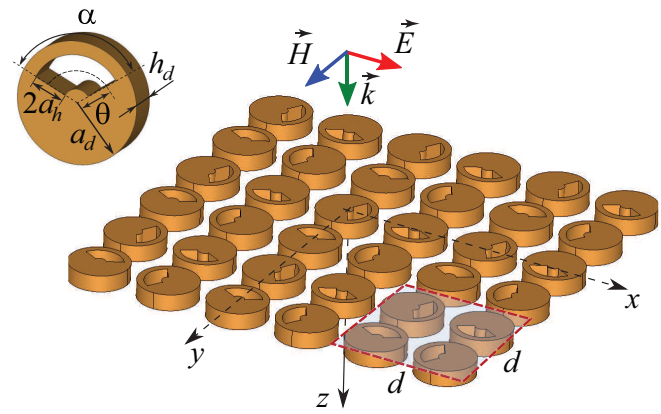

FIG. 1. Schematic view of an all-dielectric metasurface with the supercell composed of four identical particles having coaxial-sector notch. a_d and h_d are the disks radius and height, respectively, θ is the radius of the sector midline, $2a_h$ is the notch width, and α is the sector opening angle. The disks are made from a nonmagnetic dielectric having permittivity ε_d. All disks are deposited equidistantly with period d. The lattice is buried into a dielectric host having permittivity ε_s and thickness h_s to form a whole metasurface (not shown in the figure).

Next we modify the metasurface by introducing notches into disks. The point symmetry of the supercell depends on the orientation of these notches in the four disks. For the first design, symmetry of the supercell in the x-y plane is described by the group C_s (in Schöenflies notation [43]), which contains only one vertical plane of symmetry $x = 0$.

If notches are made, the resonant state discussed above for solid disks arises for the modified structure as well. Nevertheless, an additional resonance appears in the spectra of the modified structure (see also Appendix). It is related to the trapped mode as is typical for structures with a broken symmetry of particles [21].

For the first design, the trapped mode appears only in the spectra of the metasurface excited by the x-polarized wave (see Fig. 2(b) and the Supplemental Material [44]). It is distinguished on the spectral curves by the green arrows. The resonance acquires a sharp peak-and-trough (Fano) profile where extremes of transmission and reflection approach to 0 and 1 alternately, since in the simulation the losses in materials forming the metasurface are considered to be absent.

From the analysis of the polarization current and magnetic field distributions in the middle plane (x-y plane at z coordinate corresponding to the half-height of the particles) it is revealed that the identified trapped mode resembles the characteristics of the lowest transverse electric ($TE_{01\delta}$) mode of the individual cylindrical dielectric resonator (see the color maps in Fig. 2(b) and Supplemental Material [44]). The resonant frequency of the trapped mode is lower than that of the electric dipole mode, so the trapped mode appears as a peripheral lowest-frequency (red-shifted [14]) resonance. For the trapped mode, there is a specific distribution of the electromagnetic field within each particle. The polarization currents have a circular flow twisting around the particle's center, whereas the magnetic field direction in the particle centers is oriented orthogonally to the metasurface plane

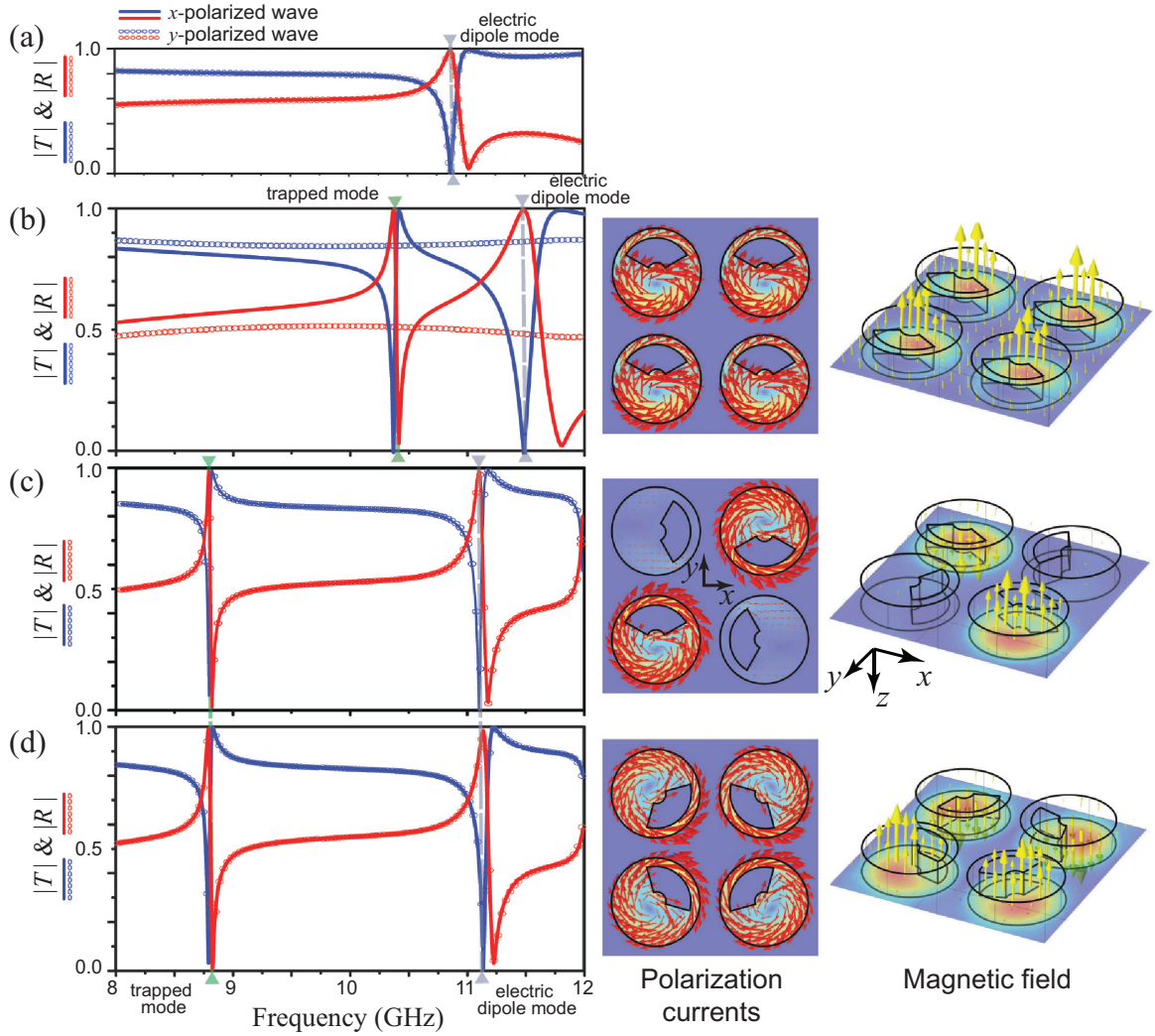

FIG. 2. Transmission (T) and reflection (R) coefficients of an all-dielectric (lossless) metasurface with the supercell composed of (a) solid disks, and particles with notches oriented with symmetry (b) C_s, (c) C_4, and (d) C_{4v}. The geometrical parameters of the disk are $a_d = 4.5$ mm, $h_d = 2.5$ mm, $\theta = 2$ mm, $a_h = 1$ mm, $\alpha = 120^\circ$, the period of lattice is $d = 22$ mm. The permittivities of disks and host are $\varepsilon_d = 24$ and $\varepsilon_s = 1.1$, respectively. The thickness of the host is $h_s = 20$ mm. The color maps demonstrate distributions of the polarization current (red arrows) and magnetic field (yellow arrows) calculated within the supercell at the resonant frequency of trapped mode excited by the x-polarized incident wave.

forming out-of-plane magnetic dipole moment. All magnetic moments induced in the metasurface are oriented in the same direction demonstrating a dynamic ferromagnetic order [45].

The most straightforward way to construct a polarization-insensitive metasurface based on the same particles is to rearrange them within the 2×2 supercells, similarly to those proposed for the split-ring-based metasurfaces [34,36–38]. For the normal wave incidence, symmetry of the supercell in the x-y plane is described by the group C_4, which consists of the fourfold axis for rotation around the z axis [Fig. 2(c)]. It is mathematically proven that for the metasurfaces whose unit cell symmetry belongs to the rotational groups C_n, for $n > 2$ there is polarization independence of the structure [46]. In Fig. 2(c) one can see that the spectral characteristics of the metasurface corresponding to excitation with two different polarizations are indeed identical.

For each polarization, the trapped mode is supported by a pair of active particles placed diagonally, while the remaining two resonators are inactive. In the color maps of Fig. 2(c) (see also Supplemental Material [44]) an active pair of particles is presented for the x-polarized wave. Another pair is active for the y-polarized wave and has the similar field distributions (are not presented here). Such distribution of active and inactive particles can be explained by the direction of the induced electric dipole moment in the notches of disks [33]. The out-of-plane magnetic moments induced in the active particles are oriented in the opposite directions resembling a dynamic antiferromagnetic order [45,47], which leads to a shift of the resonance to the low-frequency region in comparison with the C_s design.

Next it is our goal to find the polarization-insensitive configuration when all particles in the supercell are active. For the metasurface under study there is a possibility to further increase the symmetry order of the supercell via the design transition from the group C_4 to the group C_{4v}. The latter contains additionally four vertical planes of symmetry passing

through the z axis. They are $x = 0$, $y = 0$ and two diagonal planes. For this design the notches of the particles should be oriented either inward or outward the center of the supercell. These two configurations are in fact identical, since the disks are situated equidistantly in the two-dimensional lattice, and thus there is arbitrariness in the supercell choice. Remarkably, for such a design all four particles in the supercell are active ones for the waves of both orthogonal polarizations.

The spectra of the metasurface whose unit cell possesses the higher symmetry and is described by the group C_{4v} is presented in Fig. 2(d). It can be seen that in the frequency band of interest, the spectral curves for metasurfaces describing by the group C_4 and the group C_{4v} are almost the same. The corresponding field distributions at the resonant frequency are presented in the color maps of Fig. 2(d) and the Supplemental Material [44]. Although in this design all particles are active, the dynamic antiferromagnetic order of the out-of-plane magnetic moments is preserved, and therefore the resonant frequency is very close to that of the C_4 design.

III. EXPERIMENTAL VERIFICATION

In order to verify the polarization-insensitive appearance of a trapped mode, the prototypes of metasurface were fabricated and experimentally investigated in the microwave frequency range. As a dielectric material the Taizhou Wangling TP-series microwave ceramic characterized by the relative permittivity $\varepsilon_d = 24$ and loss tangent $\tan\delta_d \leqslant 1 \times 10^{-3}$ at 10 GHz has been used. The dielectric particles with the sizes mentioned in the caption of Fig. 2 were fabricated with the use of precise mechanical cutting techniques. To arrange them, an array of holes was milled in a custom holder made of a styrofoam material whose relative permittivity is $\varepsilon_s = 1.1$ and thickness of the plate is $h_s = 20.0$ mm. The metasurface prototypes were constructed of 12×12 supercells (so we used 576 particles in total) arranged in a lattice having the period $d = 22$ mm.

At the first step the transmission and reflection spectra have been measured for all the metasurface prototypes. The common technique when the measurements are performed in the radiating near-field region and then transformed to the far-field zone has been used [48]. During the investigation the prototype was fixed on the 2.0 m distance from a rectangular linearly polarized broadband horn antenna as shown in Fig. 3(a). The antenna generates a quasi-plane-wave with required polarization. The beam width at the frequency of 9 GHz is 500 mm with the level of -3 dB. The antenna is connected to the port of the Vector Network Analyzer (VNA) Agilent E8362C by a 50 Ohm coaxial cable.

An electrically small dipole probe oriented in parallel to the metasurface plane and connected to the second port of the VNA was used to detect the near electric field. The scan area (220×220 mm) was chosen a little smaller than the sample size in order to reduce the effects of the sample edges on the measurement results. During the measurements the probe was automatically moved in the x-y plane over the scan area with a 5 mm step at the distance of 30 mm above the prototype surface. At each probe position both amplitude and phase of the transverse component of the electric field were sampled in the frequency range of interest (8–12 GHz). The same values

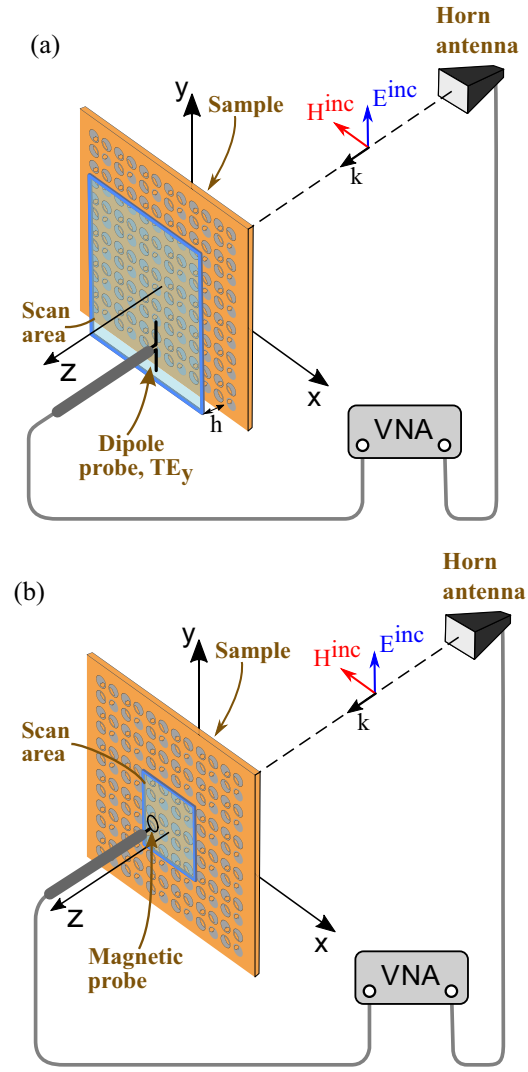

FIG. 3. Experimental setups for measurements of the (a) transmission and reflection spectra and (b) magnetic near-field distribution.

of the electric field in the absence of the prototype were measured as a reference and the postprocessing procedure was performed to obtain the transmission coefficient [48]. The similar procedure has been performed to measure the reflection coefficient excepting the scanning of the field above a metal plate placed instead of the metasurface prototype as a reference for the postprocessing procedure.

The measured transmission and reflection coefficients for all proposed designs are depicted in Fig. 4 in comparison to the results of numerical simulation of actual metasurfaces. One can conclude that the measured data repeat well the simulated results. To not overload the picture in Figs. 4(b) and 4(c) we presented curves only for the x-polarized wave, making sure that the spectra are identical for the waves of both orthogonal polarizations having carried out the corresponding measurements.

At the next step we have experimentally studied the near-field distribution of the metasurfaces. According to the results of our numerical simulations the electric field is mostly con-

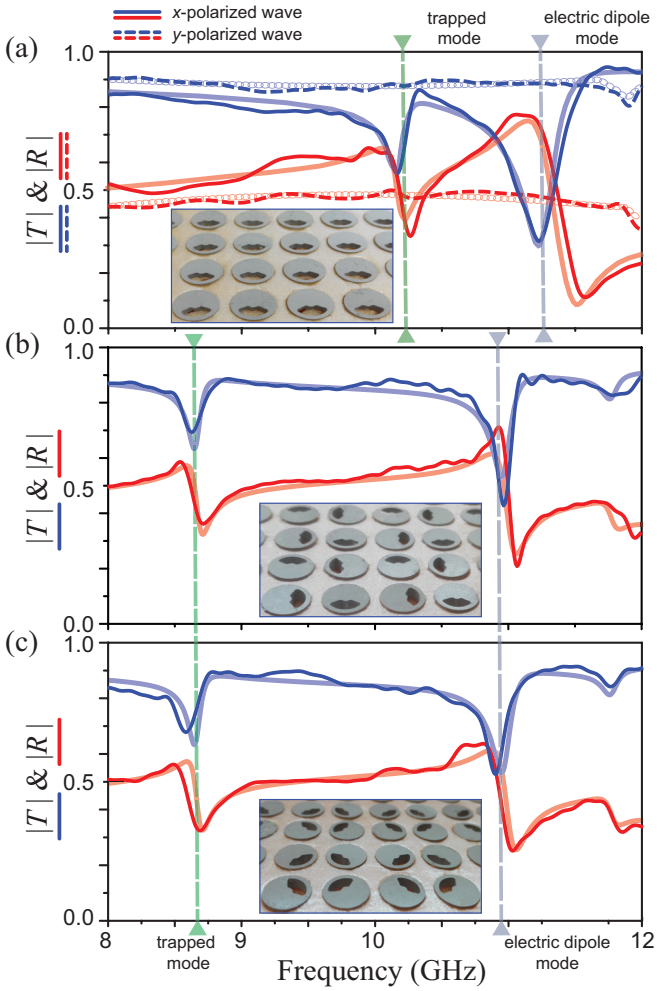

FIG. 4. Simulated (pale lines) and measured (bright lines) transmission and reflection coefficients of the all-dielectric metasurface with the supercell composed of particles oriented with symmetry (a) C_s, (b) C_4, and (c) C_{4v}. In the simulation actual material losses ($\tan\delta = 1 \times 10^{-3}$) in ceramic disks are taken into account, while the substrate is modeled as a lossless dielectric. The insets demonstrate fragments of the metasurface prototypes. The geometrical parameters of the metasurface are the same as in Fig. 2.

centrated inside the particles, whereas the magnetic field is penetrating out of the resonators. Moreover, the magnetic moments are orthogonally oriented to the metasurface plane and demonstrate different patterns with respect to the particular resonator orderings. Thus, we have measured the magnetic near-field distribution for all the proposed designs. For that purpose we slightly changed the experimental setup. We used a small magnetic probe placed in the x-y plane instead of the electric one [see Fig. 3(b)]. The normal component (H_z) of the magnetic near field has been scanned over the area of 20×44 mm with 1 mm step covering 1×2 supercells. The near-field scanning was performed on the distance of 1 mm above the metasurface prototypes. The color maps of the measured near-field distribution confirming discussed above trapped mode resonant conditions and orientations of the out-of-plane magnetic moments are shown in Fig. 5.

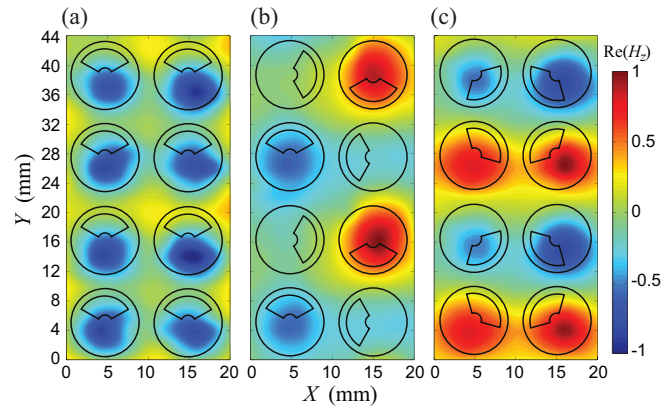

FIG. 5. Measured real part of the H_z component of the magnetic near-field (out-of-plane magnetic moments) at the corresponding resonant frequency of trapped mode excited by the x-polarized incident wave in the all-dielectric metasurface with the supercell composed of particles oriented with symmetry (a) C_s, (b) C_4, and (c) C_{4v}.

IV. CONCLUSIONS

In conclusion, we have studied the appearance of a trapped mode in several polarization-insensitive designs of the all-dielectric metasurface under the normal wave incidence condition. The super-cell configuration for these designs is related to the symmetry groups C_s, C_4, and C_{4v}. Three different distributions of the magnetic moments are found to exist within the supercell, which resemble either ferromagnetic or antiferromagnetic order.

Similar to characteristics of the Mie-type modes, the spectral line of the trapped mode acquires a sharp peak-and-trough profile, whereas the quality factor of such resonance can be much higher than that of the Mie-type modes. Moreover, the quality factor of such trapped mode is fully controlled by the degree of structural asymmetry. The distinctive feature of the trapped mode is that it is an alone-standing lowest-frequency resonance (i.e., in terms of wavelength it acquires a giant red shift), and, thus, this resonance can be easily recognized and controlled among other resonances in the spectrum.

Although in our designs the particles with coaxial-sector notch in the shape of a smile are used, we argue the considered effects have a common nature and will also exist in particles with holes of a simpler shape, for example, in resonators with an off-centered round or rectangular hole that are easier to fabricate at the nanoscale. We believe that proposed designs can be useful in highly sensitive sensors, filters, and strong light matter interaction applications where the polarization-insensitivity feature provides additional benefits.

ACKNOWLEDGMENTS

The experimental investigation of the reflection and transmission coefficients in the microwave frequency range has been supported by RSF (Grant No. 17-19-01731). S.X. acknowledges support from the National Key Research and Development Program of China and National Natural Science Foundation of China (NSFC) under Grant No. 61805097. V.D. thanks Brazilian agency CNPq for financial support. V.R.T. acknowledges Jilin University's hospitality and financial

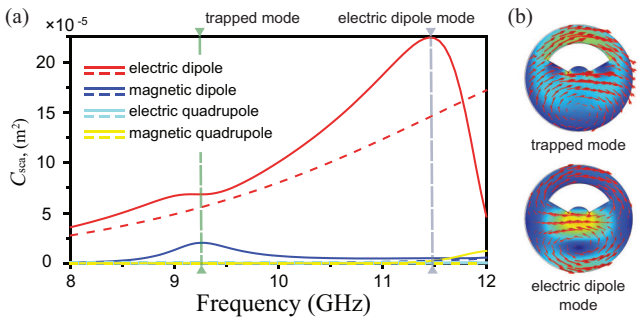

FIG. 6. (a) Contributions of four lowest-order multipole moments to the scattering cross section of a single particle irradiated by either *x*-polarized (solid lines) or *y*-polarized (dashed lines) wave, and (b) cross-section patterns of electric field distribution, which are calculated at the corresponding frequencies of the trapped mode and electric dipole mode resonances.

support, and also thanks Yu. S. Kivshar for useful discussions and suggestions.

APPENDIX: SCATTERING CROSS SECTION OF A SINGLE PARTICLE

We performed simulations of the electromagnetic wave scattering by an isolated particle with a coaxial-sector notch in order to prove that the discussed resonant state (trapped mode) is inherent to an individual dielectric resonator rather than produced by the electromagnetic coupling between them. As an exciting radiation, a plane electromagnetic wave having linear polarization is supposed. We consider incidence of waves of both orthogonal polarizations (*x*-polarized and *y*-polarized waves). The wave incidents along the axis of the disk (frontal excitation). The sum of the contributions from different multipole moments is written as [49]

$$C_{\text{sca}}^{\text{total}} = C_{\text{sca}}^{p} + C_{\text{sca}}^{m} + C_{\text{sca}}^{Q_e} + C_{\text{sca}}^{Q_m} + \ldots, \qquad \text{(A1)}$$

where, C_{sca}^{p}, C_{sca}^{m}, $C_{\text{sca}}^{Q_e}$, $C_{\text{sca}}^{Q_m}$ are the contributions to scattering cross section from electric dipole, magnetic dipole, electric quadrupole, and magnetic quadrupole, respectively.

In Fig. 6 the contribution of four lowest-order multipole (dipole and quadrupole) moments to the scattering cross section of the given particle irradiated by the *x*-polarized and *y*-polarized wave are shown. In the frequency band of interest, along with the resonance related to the electric dipole moment, an additional low-frequency resonance arises in the scattering cross section of the particle. It only appears in the response on excitation by the *x*-polarized wave, so it is peculiar to the particle with broken symmetry. We identify it as a trapped mode. Both electric and magnetic dipole moments contribute to this mode.

[1] N. I. Zheludev, Science **348**, 973 (2015).
[2] N. I. Zheludev and Y. S. Kivshar, Nature Mater. **11**, 917 (2012).
[3] S. Kruk and Y. Kivshar, ACS Photonics **4**, 2638 (2017).
[4] Q. Zhao, J. Zhou, F. Zhang, and D. Lippens, Mater. Today **12**, 60 (2009).
[5] S. Jahani and Z. Jacob, Nature Nanotechnol. **11**, 23 (2016).
[6] D. G. Baranov, D. A. Zuev, S. I. Lepeshov, O. V. Kotov, A. E. Krasnok, A. B. Evlyukhin, and B. N. Chichkov, Optica **4**, 814 (2017).
[7] A. Trubin, *Lattices of Dielectric Resonators*, Springer Series in Advanced Microelectronics, Vol. 53 (Springer Cham, Heidelberg, 2016).
[8] C. F. Bohren and D. R. Huffmann, *Absorption and Scattering of Light by Small Particles* (Wiley-Interscience, New York, 2010).
[9] M. Decker, I. Staude, M. Falkner, J. Dominguez, D. N. Neshev, I. Brener, T. Pertsch, and Y. S. Kivshar, Adv. Opt. Mater. **3**, 813 (2015).
[10] O. Tsilipakos, A. C. Tasolamprou, T. Koschny, M. Kafesaki, E. N. Economou, and C. M. Soukoulis, Adv. Opt. Mater. **6**, 1800633 (2018).
[11] P. Spinelli, M. A. Verschuuren, and A. Polman, Nature Commun. **3**, 692 (2012).
[12] X. Liu, K. Fan, I. V. Shadrivov, and W. J. Padilla, Opt. Express **25**, 191 (2017).
[13] N. Bontempi, K. E. Chong, H. W. Orton, I. Staude, D.-Y. Choi, I. Alessandri, Y. S. Kivshar, and D. N. Neshev, Nanoscale **9**, 4972 (2017).
[14] V. V. Khardikov, E. O. Iarko, and S. L. Prosvirnin, J. Opt. **14**, 035103 (2012).
[15] J. Zhang, K. F. MacDonald, and N. I. Zheludev, Opt. Express **21**, 26721 (2013).
[16] S. Campione, S. Liu, L. I. Basilio, L. K. Warne, W. L. Langston, T. S. Luk, J. R. Wendt, J. L. Reno, G. A. Keeler, I. Brener, and M. B. Sinclair, ACS Photonics **3**, 2362 (2016).
[17] V. R. Tuz, V. V. Khardikov, A. S. Kupriianov, K. L. Domina, S. Xu, H. Wang, and H.-B. Sun, Opt. Express **26**, 2905 (2018).
[18] C. Cui, C. Zhou, S. Yuan, X. Qiu, L. Zhu, Y. Wang, Y. Li, J. Song, Q. Huang, Y. Wang, C. Zeng, and J. Xia, ACS Photonics **5**, 4074 (2018).
[19] R. Singh, C. Rockstuhl, F. Lederer, and W. Zhang, Phys. Rev. B **79**, 085111 (2009).
[20] S. Prosvirnin and S. Zouhdi, in *Advances in Electromagnetics of Complex Media and Metamaterials*, edited by S. Zouhdi and M. Arsalane (Kluwer Academic Publishers, Dordrecht, 2003), pp. 281–290.
[21] V. A. Fedotov, M. Rose, S. L. Prosvirnin, N. Papasimakis, and N. I. Zheludev, Phys. Rev. Lett. **99**, 147401 (2007).
[22] C. W. Hsu, B. Zhen, A. D. Stone, J. D. Joannopoulos, and M. Soljačić, Nat. Rev. Mater. **1**, 16048 (2016).
[23] K. Koshelev, S. Lepeshov, M. Liu, A. Bogdanov, and Y. Kivshar, Phys. Rev. Lett. **121**, 193903 (2018).
[24] N. Papasimakis, Y. H. Fu, V. A. Fedotov, S. L. Prosvirnin, D. P. Tsai, and N. I. Zheludev, Appl. Phys. Lett. **94**, 211902 (2009).
[25] M. N. Kawakatsu, V. A. Dmitriev, and S. L. Prosvirnin, J. Electromagn. Waves Appl. **24**, 261 (2010).
[26] I. A. I. Al-Naib, C. Jansen, N. Born, and M. Koch, Appl. Phys. Lett. **98**, 091107 (2011).
[27] V. R. Tuz and S. L. Prosvirnin, Eur. Phys. J. Appl. Phys. **56**, 30401 (2011).

[28] V. R. Tuz, V. S. Butylkin, and S. L. Prosvirnin, J. Opt. **14**, 045102 (2012).
[29] F. Meng, Q. Wu, D. Erni, K. Wu, and J. Lee, IEEE Trans. Microw. Theory Tech. **60**, 3013 (2012).
[30] P. V. Tuong, J. W. Park, J. Y. Rhee, K. W. Kim, W. H. Jang, H. Cheong, and Y. P. Lee, Appl. Phys. Lett. **102**, 081122 (2013).
[31] S. W. Yu, J. H. Shi, Z. Zhu, R. Liu, and C. Y. Guan, J. Opt. **15**, 075103 (2013).
[32] F. Zhang, Q. Zhao, J. Zhou, and S. Wang, Opt. Express **21**, 19675 (2013).
[33] A. Jain, P. Moitra, T. Koschny, J. Valentine, and C. M. Soukoulis, Adv. Opt. Mater. **3**, 1431 (2015).
[34] A. Sayanskiy, M. Danaeifar, P. Kapitanova, and A. E. Miroshnichenko, Adv. Opt. Mater. **6**, 1800302 (2018).
[35] C. S. Lim, M. H. Hong, Z. C. Chen, N. R. Han, B. Luk'yanchuk, and T. C. Chong, Opt. Express **18**, 12421 (2010).
[36] I. Al-Naib, R. Singh, C. Rockstuhl, F. Lederer, S. Delprat, D. Rocheleau, M. Chaker, T. Ozaki, and R. Morandotti, Appl. Phys. Lett. **101**, 071108 (2012).
[37] N. Born, I. Al-Naib, M. Scheller, C. Jansen, J. V. Moloney, and M. Koch, in *39th International Conference on Infrared, Millimeter, and Terahertz Waves (IRMMW-THz),* 2014, pp. 1–2.
[38] L. Wu, Z. Yang, M. Zhao, Y. Zheng, J. Duan, and X. Yuan, Opt. Express **22**, 14588 (2014).
[39] V. R. Tuz, V. V. Khardikov, and Y. S. Kivshar, ACS Photonics **5**, 1871 (2018).
[40] V. Dmitriev, Metamaterials **5**, 141 (2011).
[41] V. Dmitriev, IEEE Trans. Antennas Propag. **61**, 185 (2013).
[42] "Frequency selective surface, periodic complementary split ring resonator", Comsol Application Gallery ID: 15711.
[43] A. A. Barybin and V. A. Dmitriev, *Modern Electrodynamics and Coupled-Mode Theory: Application to Guided-Wave Optics* (Rinton Press, Princeton, 2002).
[44] See Supplemental Material at http://link.aps.org/supplemental/10.1103/PhysRevB.99.085306 for animation representing the dynamic of the electromagnetic near field within the supercell of the all-dielectric metasurface. They correspond to those presented in Fig. 2 of the paper.
[45] M. Decker, S. Burger, S. Linden, and M. Wegener, Phys. Rev. B **80**, 193102 (2009).
[46] A. Mackay, Electron. Lett. **25**, 1624 (1989).
[47] M. Decker, S. Linden, and M. Wegener, Opt. Lett. **34**, 1579 (2009).
[48] R. C. Johnson, H. A. Ecker, and J. S. Hollis, Proc. IEEE **61**, 1668 (1973).
[49] J. D. Jackson, *Classical Electrodynamics*, 3rd ed. (John Wiley & Sons, New York, 1999).